Quantitative Magnetization Transfer Mapping of Bound Protons in Multiple Sclerosis

D. Tozer,* A. Ramani, G.J. Barker, G.R. Davies, D.H. Miller, and P.S. Tofts

Quantitative analysis of magnetization transfer images has the potential to allow a more thorough characterization of the protons, both bound and free, in a tissue by extracting a number of parameters relating to the NMR properties of the protons and their local environment. This work develops previously presented techniques to produce estimates of parameters such as the bound proton fraction, f, and the transverse relaxation time of the bound pool, T_{2B}, for the whole brain in a clinically acceptable imaging time. This is achieved by limiting the number of data collected (typically to 10); to collect 28 5-mm slices with a reconstructed resolution of 0.94 × 0.94 mm. The protocol takes 82 sec per data point. The fitting technique is assessed against previous work and for fitting failures. Maps and analysis are presented from a group of seven controls and 20 multiple sclerosis patients. The maps show that the parameters are sensitive to tissue-specific differences and can detect pathological change within lesions. Statistically significant differences in parameters such as T_{2B} and f are seen between normal-appearing white matter, multiple sclerosis lesions, and control white matter. Whole-brain histograms of these parameters are also presented, showing differences between patients and controls. Magn Reson Med 50:83–91, 2003. © 2003 Wiley-Liss, Inc.

Key words: magnetization transfer; multiple sclerosis; quantitative analysis; bound proton; histogram

Magnetization transfer (MT) imaging is possible due to the exchange of magnetization between two or more groups of spins by either chemical exchange or cross-relaxation (1,2). In most tissues the relaxation time of the group of spins associated with macromolecules makes them invisible using conventional MR imaging; however, they can be indirectly imaged using MT. Most commonly a two-pool model of living tissue is used, as described in (3), although some investigators have proposed a more complex three-pool model (4).

The phenomenon of MT is described in detail in Refs. (5–8), but simply involves the application of off-resonance RF radiation to saturate the protons in the bound pool, which are then exchanged to the free pool. This was first demonstrated on animal models by Wolff and Balaban (9). The effect is mostly used to produce an MT ratio (MTR) (10), which can be compared and is reproducible among subjects; however, the MTR is heavily scanner- and sequence-dependent (11,12).

MT is potentially a very useful tool for the study of multiple sclerosis (MS) because of the changes seen in the white matter: as a lesion is formed, demyelination and axonal loss both occur which will alter the structure of the brain tissue. This changes the relative sizes of the bound and free pools which affects the MTR. These changes have been widely studied using conventional region of interest (ROI) (13,14) and more complex whole-brain histogram studies (15,16). However, the MTR is a combination of physiological factors, such as the relaxation times of the pools and sequence-dependent parameters such as the frequency of the saturation pulse. Useful as it may be, there are more fundamental properties of the tissue that underlie the MTR.

Quantitative analysis of MT has been developed over the last 10 years or so and a number of imaging methods have been developed. Henkelman et al. (17) were among the first to incorporate non-Bloch behavior into the mathematical description of the MT phenomenon by the application of non-Lorentzian lineshapes for the bound pool. Similar techniques have yielded one or more quantitative parameters with various saturation techniques (18,19). Although the application of quantitative MT (qMT) in vivo is a relatively novel area, there has been some work done in the general area. The initial work by Henkelman et al. (17) and Morrison and Henkelman (20) was carried out on various samples such as agar jelly and fresh samples of bovine muscle and bovine white matter.

Similar techniques have been applied by a number of groups to produce a full set of parameters for the MT phenomenon (21–23).

Of particular interest are the results produced in this group by Ramani et al. (24) and by Sled and Pike (25), who both presented preliminary data from MS patients. This work has suggested that a reduction in the bound proton fraction and the T_2 of the bound pool is seen in MS lesions compared to normal-appearing white matter (NAWM).

The purpose of this work is to show that the production of both maps and histograms of the various parameters detailed in the model can be achieved by the application of a robust, reproducible fitting routine, which can lead to detailed analysis of the whole brain in a clinically acceptable time.

THEORY

The theory of qMT has been covered in detail elsewhere and a complete derivation will not be given here. The refinements made by Ramani et al. (24) to the model proposed by Henkelman et al. (17), shown in Eq. [1], will be described, but the initial modification of the Bloch equations to take account of the saturating radiation used in MT will not be detailed.

NMR Research Unit, Department of Neuroinflammation, Institute of Neurology, University College London, London, UK.

*Correspondence to: Dr. Daniel Tozer, NMR Research Unit, Institute of Neurology, Queen Square, London WC1N 3BG, UK.

Received 19 September 2002; revised 16 January 2003; accepted 19 February 2003.

DOI 10.1002/mrm.10514
Published online in Wiley InterScience (www.interscience.wiley.com).

$$S = gM_0^A \times \left(\frac{R_B\left[\frac{RM_0^B}{R_A}\right] + R_{RFB} + R_B + RM_0^A}{\left[\frac{RM_0^B}{R_A}\right](R_B + R_{RFB}) + \left(1 + \left[\frac{\omega_1}{2\pi\Delta f}\right]^2\left[\frac{1}{R_A T_2^A}\right]\right)(R_{RFB} + R_B + RM_0^A)} \right). \quad [1]$$

In this equation, S is the signal intensity obtained from a volume of interest, g is a scaling factor based on the electronic settings of the scanner, M_0^A and M_0^B are the native magnetizations of the free and bound pools, respectively, R_A and R_B are the longitudinal relaxation rates of the two pools, R is a measure of the coupling of the two pools, T_2^A is the transverse relaxation time of the free pool, R_{RFB} is a factor which represents the lineshape of the bound pool, which introduces the transverse relaxation time of the bound pool to the model, the form of this will be discussed later, ω_1 is the amplitude of the continuous saturation pulse, and Δf is the offset frequency of the pulse. Equation [1] differs from Henkelman's only in that the data are not normalized, so M_0^A is still explicitly included.

To take account of the MT pulsed experiment used here, a continuous wave power equivalent amplitude of the MT pulse (ω_{CWPE}) can be calculated using the effective saturation power, assumed to be equivalent to the mean saturating power of a pulse and the technique presented by Ramani and Tofts (26). Information about the pulse shape, duration, its peak magnetic field and the interpulse interval (TR′) is combined to produce a value for the amplitude of a continuous wave with the same mean power; this is shown in Eq. [2]:

$$\omega_{CWPE} = \gamma B_{ICWPE} = \gamma\sqrt{P_{sat}} = p_2\theta^2/p_1^2 TR'\gamma\tau_{sat} \quad [2]$$

where p_1 and p_2 are geometric factors dependent on the pulse shape; more specifically, p_1 is the ratio of the area of the pulse to a rectangular pulse of the same duration and peak amplitude and p_2 is the ratio of the square of the pulse area to the square of the area of the same rectangular pulse, θ is the effective tip angle of the pulse if applied on resonance (in rads), τ_{sat} is the length of the MT pulse, and P_{sat} is the mean square saturating field. The values of TR′ routinely used here are within the range of times validated by Ramani and Tofts (26) from comparison of theoretical and observed MTR values justifying the use of the CWPE correction here.

Although the Bloch equations give rise to a Lorentzian lineshape for both the free and bound pools, it has been shown that this does not adequately fit the data in a number of samples (17,20) such as agar gel and fresh bovine white matter; instead, Gaussian and super-Lorentzian lineshapes, respectively, were found to give better fits. The general form of the lineshape, G, and the specifics of the two in question are shown in Eqs. [3]–[5]:

$$R_{RFB} = \pi\omega_{CWPE}^2 G(2\pi\Delta f) \quad [3]$$

$$G_{Gauss}(2\pi\Delta f) = \frac{T_2}{\sqrt{2\pi}}\exp -\left(\frac{(2\pi\Delta f T_2)^2}{2}\right) \quad [4]$$

$$G_{SL}(2\pi\Delta f) = \int_0^{\pi/2} d\theta \sin\theta \sqrt{\frac{2}{\pi}}\frac{T_2}{(|3\cos^2\theta - 1|)} e^{-2[2\pi\Delta f T_2/|3\cos^2\theta - 1|]^2}. \quad [5]$$

The T_2 of a solid depends on the orientation of the spins with respect to B_0, so as regards the bound pool, which is semisolid in nature, it is wrong to talk about the T_2 of this pool as a single and invariant value. This can affect the estimates of all the parameters in the model, but in particular T_{2B}, as the signal seen in a voxel will depend on the orientation of the semisolid spins in that voxel, which is not modeled for, rather than simply the value of T_{2B}. The super-Lorentzian lineshape is used in an attempt to overcome this, as the T_2 quoted is an average over all orientations of the relaxation time of the semisolid protons, suggesting that it might be the most appropriate lineshape to use.

The model shown in Eq. [1] was also modified slightly to produce a physically meaningful parameter, the bound proton fraction, f. This was achieved by using the definition of f given by Ramani et al. (24):

$$f = M_0^B/(M_0^A + M_0^B). \quad [6]$$

By substituting for M_0^B into Eq. [1], which can then be rewritten as shown in Eq. [7]:

$$S = gM_0^A \times \left(\frac{R_B\left[\frac{RM_0^A f}{R_A(1-f)}\right] + R_{RFB} + R_B + RM_0^A}{\left[\frac{RM_0^A f}{R_A(1-f)}\right](R_B + R_{RFB}) + \left(1 + \left[\frac{\omega_{CWPE}}{2\pi\Delta f}\right]^2\left[\frac{1}{R_A T_2^A}\right]\right)(R_{RFB} + R_B + RM_0^A)} \right) \quad [7]$$

a set of six parameters can be obtained from the data; these are, gM_0^A, R_B, RM_0^A, $f/R_A(1-f)$, $1/R_A T_2^A$, and through the lineshape, R_{RFB}, T_{2B}.

From the estimates of $f/R_A(1-f)$ and RM_0^A and the corresponding value of R_{1obs}, the inverse of the value taken from the calculated T_1 map Eq. [8], also from Henkelman's work (17), can be used to obtain an estimate of R_A from which a value for f can be calculated:

$$R_A = \frac{R_{1obs}}{1 + \left(\frac{\frac{RM_0^A f}{(1-f)R_A}(R_B - R_{1obs})}{(R_B - R_{1obs}) + RM_0^A}\right)}. \quad [8]$$

SUBJECTS AND METHODS

Imaging Methods and Subjects

A 2D spoiled gradient echo sequence previously described in Ref. 24 with the following parameters: TR/TE = 1140/12 ms, excitation flip angle = 25°, acquisition matrix = 256 × 128, reconstructed matrix size = 256 × 256, number of excitations = 0.75, i.e., partial filling of *k*-space, FOV =

Table 1
Amplitudes and Offset Frequencies of the MT Pulse Used in These Experiments

Flip Angle°	ω_{CWPE} (rad s^{-1})	Δf (Hz)
212	185	1000
212	185	2500
212	185	7500
434	378	1000
434	378	3500
434	378	15000
843	735	1000
843	735	2500
843	735	5000
843	735	7500

24 × 24 cm with $\frac{3}{4}$ FOV in the phase direction was implemented with 28 5-mm contiguous slices giving whole-brain coverage. All 28 slices were acquired in a single TR so the MT pulse repetition time, or TR′, was 41 ms. A small excitation flip angle was chosen to minimize the T_1 weighting of the images while retaining an acceptable signal-to-noise ratio (SNR). The sequence was sensitized to MT by the application of a Gaussian MT pulse, with a duration of 14.6 ms and of a given amplitude and frequency offset, before the 25° pulse. Each set of 28 images takes 1 min, 22 sec to acquire and the sequence is repeated a number of times dependent on the number of data points chosen by the operator.

Although any number of data points can be obtained, time considerations limit the practicality of taking many points; for the examples described here it was decided to have 10 combinations of power and offset frequency. This keeps the total imaging time, including all localizers and the T_1 measurement described below, to around 45–50 min, which is clinically acceptable, while allowing enough degrees of freedom to calculate parameter estimates. It has been shown (17) that choosing n offset frequencies and 1 amplitude does not provide enough information to adequately fit the model, so it was decided to use 3 amplitudes with 3, 3, and 4 offset frequencies; the values of these are shown in Table 1. The MT pulse parameters were chosen with regard to SAR limitations and a desire to cover as wide a range of offset frequencies as possible, while ensuring that the region in which the signal intensity is expected to change the most is well covered.

The values for ω_{CWPE} were calculated using the CWPE calculation described above. Figure 1 shows example sig-

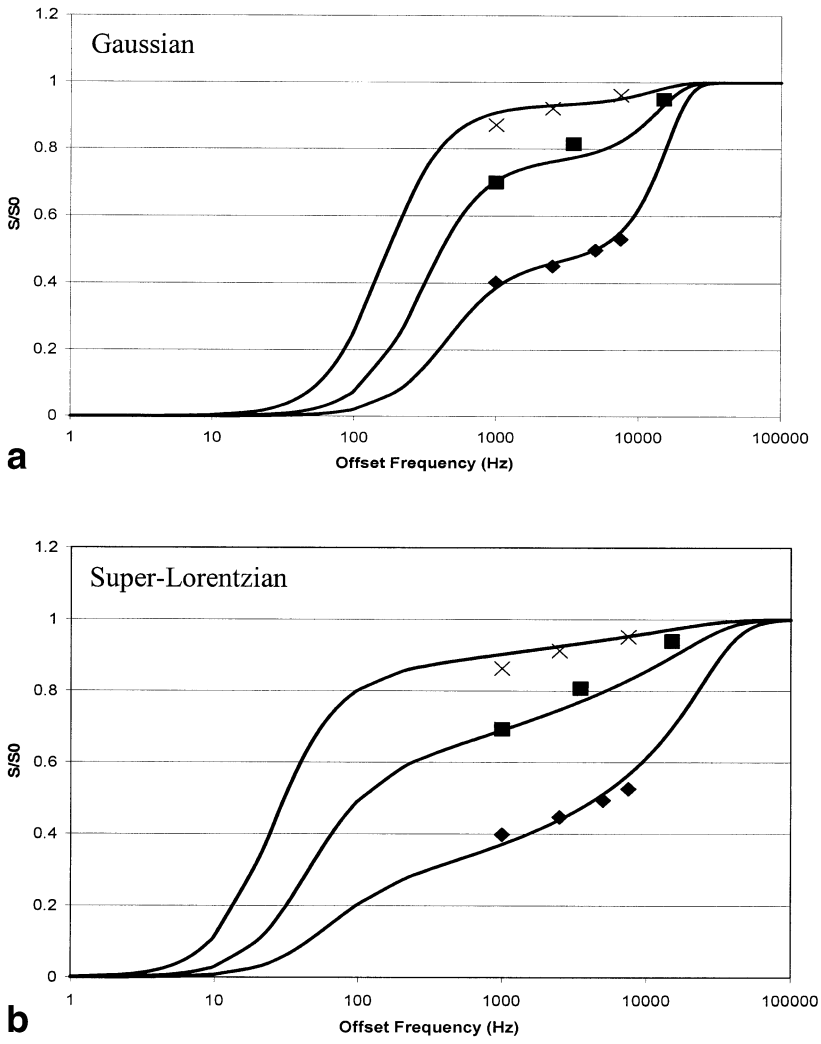

FIG. 1. Typical graphs from a region drawn in white matter in a control subject. **a:** The data fitted with a Gaussian lineshape. **b:** The same but using a super-Lorentzian lineshape. As can be seen, the Gaussian gives the better fit, with a reduction of ~35% in the SSQ. In both graphs the marked points are the data collected in the experiment at each power and the three lines represent the three powers used in the experiment 184.8 (×), 378.3 (■), and 734.8 (◆) rads/s from top to bottom.

nal intensity curves calculated from the model from a region drawn in white matter in a control; the symbols here indicate the offset frequencies chosen for each power and shows that these values give good coverage of the pulse amplitude curves in the region in which they are changing the most when a Gaussian lineshape is used. Although for a super-Lorentzian lineshape the coverage is not so good, there is still a reasonable change of signal in this range. Images were not acquired at low offset frequencies, as the closer the frequency of the offset frequency to the resonant frequency of the sample the greater the signal lost due to direct saturation of the free pool, resulting in low SNR images.

A dataset which allows the calculation of T_1 maps using the method described by Parker et al. (27) was acquired at the same locations.

All subjects were imaged using a T_2-weighted dataset used to calculate T_2 lesion load and exclude lesions in controls, and were also imaged using a conventional T_1 weighted sequence to obtain a T_1 lesion load.

Imaging was performed on a group of seven control subjects (average age ± SD 31 ± 6 years) with no history of neurological conditions and a group of 20 MS patients (average age 45 ± 9 years, average expanded disability status scale 3 (range 1–6.5), average duration of disease 11 years (range 1–32)). Fourteen of the patients had relapsing remitting MS and two of the other six each had primary progressive, secondary progressive, and benign MS. One of the controls was scanned on two separate occasions to test the reproducibility of the technique. The study was approved by the ethics committee of the National Hospital for Neurology and Neurosurgery and informed consent of all subjects was obtained.

Data Analysis

A 280 image dataset was produced for each patient, consisting of 28 slices for each of the 10 MT pulse combinations shown in Table 1. The work presented by Ramani et al. (24) and Henkelman et al. (17) suggested that the parameter R_B be fixed, as the residual sum of squares (SSQ) is insensitive to R_B and an accurate value cannot be determined. The parameter was also fixed in this work, as in the other work mentioned, equal to 1 s^{-1}, to save the time of fitting for an extra, unhelpful parameter. When this variable was fitted for the parameters, gM_0^A and T_{2B} were independent of it, but $f/R_A(1-f)$ and $1/R_A T_{2A}$ did vary. Although it is unlikely that this value is a good estimate of the longitudinal relaxation of the bound pool, by fixing it a source of variation in the latter two parameters is removed, allowing for their consistent estimation. Although this may introduce bias and mean that the values obtained are not physically accurate, they are more reliable, which is important for diagnostic purposes. This modified model was then fitted to the data to produce estimates of the five parameters, gM_0^A, RM_O^A, $1/R_A T_2^A$, $f/(R_A(1-f))$, and T_2^B (through the lineshape R_{RFB}). In addition, for comparison, the MTR was also estimated using the most heavily weighted set of MT images ($\omega = 735$ rad s^{-1}, $\Delta f = 1000$ Hz) and the least heavily weighted set ($\omega = 185$ rad s^{-1}, $\Delta f = 7500$ Hz).

Before fitting registration of the 10 sets of 28 MT-weighted images and the images used for T_1 calculation was carried out using the normalized Mutual Information algorithm developed by Studholme et al. (28). A simple threshold was used to exclude pixels containing only background noise, reducing the number of pixels to be fitted by 75%.

The fitting was carried out using a least squares minimization method algorithm from the Numerical Algorithms Group (NAG) (29,30). The parameters were all constrained to be positive, as a negative value for any parameter would be physically unrealistic. Estimates of the various parameters were obtained using both an ROI approach, based on signal intensities obtained from the raw data within regions placed in the brain tissues with reference to the T_2- and T_1-weighted images, and on a mapping basis, where values were calculated for each individual pixel. From these estimates comparisons of the parameters from tissues in the patients and controls were made using, where appropriate, Student's paired and independent samples *t*-tests.

The issue of which lineshape to use for the bound protons was resolved by fitting a subset of the subjects with Gaussian, Lorentzian, and super-Lorentzian lineshapes and comparing the goodness of fit for three major tissue types, white matter, gray matter, and MS lesions.

Whole-brain histograms were calculated from the parameter maps produced, including the MTR. The T_1 maps were used to create a mask of the cerebro-spinal fluid (CSF), which was then applied to the various parameter maps which were calculated from the registered images. Normalized histograms were then calculated and a simple analysis of the major features was performed.

RESULTS

Performance of Fitting

For both the ROI and pixel-by-pixel analysis, the Gaussian lineshape was found to give the best fit, with the super-Lorentzian giving the next best, and the Lorentzian the worst for all datasets in the subset tested in all three major brain tissues. An average reduction in the SSQ of ~20% was seen using the Gaussian lineshape compared with the super-Lorentzian. Typical examples of the fitted curves are shown in Fig. 1, where it can be seen that the super-Lorentzian lineshape does not result in as good a fit as the Gaussian.

The time taken to fit each dataset varied on the number of iterations required to reach convergence, and although some ROIs took 2–3 sec to converge, many took substantially less than a second. This was also the case for each pixel in the pixel-by-pixel analysis, so a dataset with 28 slices took between 4 and 48 hr to run on an ULTRA 10 workstation (Sun Microsystems, Santa Clara, CA, USA).

Analysis of the data with both an ROI and pixel-by-pixel approach yielded good quality fits and physically sensible values for the parameters; however, all values quoted here are those obtained using the ROI approach. Using the following definition of the residual deviation per point ($\sigma = \sqrt{}$(sum of squares)/(number of data points–number of parameters)) and noting that the SSQ must be normalized to gM_0^A to make it comparable to the figures found in Ref. 20, typical values for σ were found that ranged between

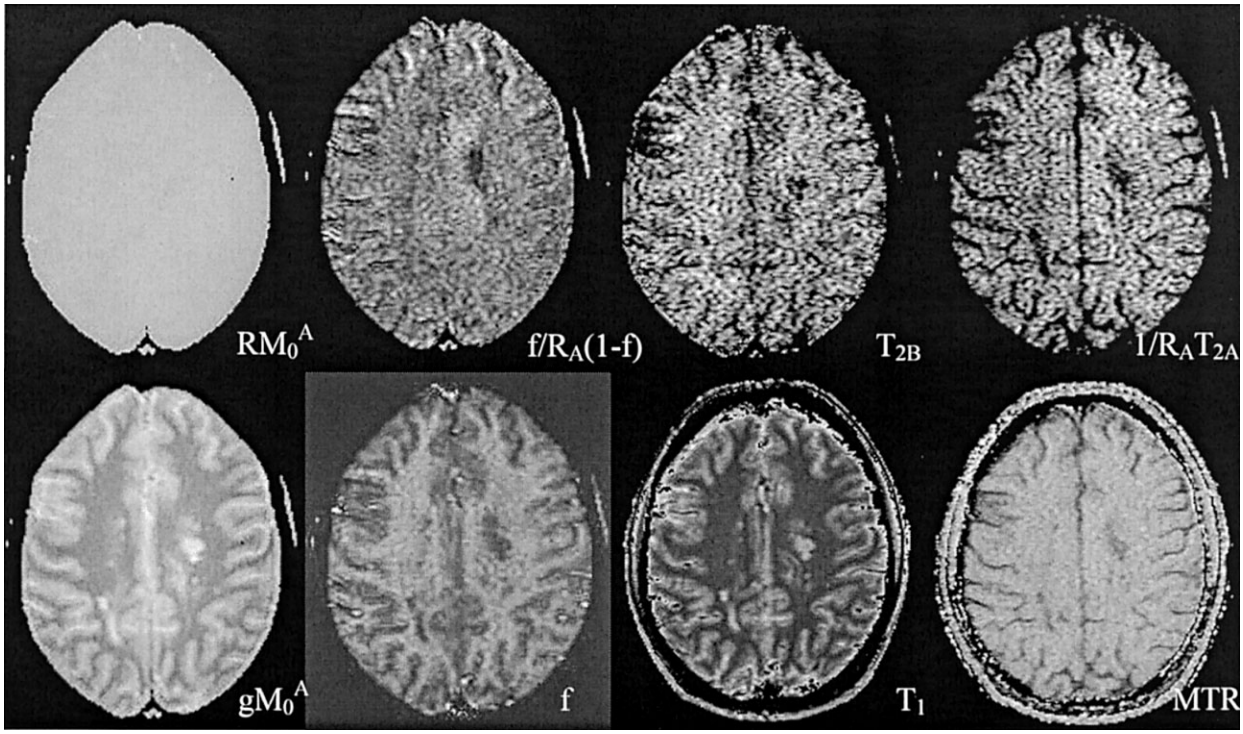

FIG. 2. A series of parameter maps obtained from an MS patient. As can be seen, the lesions visible on gM_0^A in the left centrum semiovale and posterior right of the brain are visible particularly well on $1/R_A T_{2A}$ and f, and also to a lesser extent on $f/R_A(1-f)$ and T_{2B}. The T_1 and MTR maps also show these lesions, but the shape of the left centrum semiovale lesion in particular seems to vary—it appears bigger on the f and $1/R\ R_A T_{2A}$ maps than on the T_1 map, indicating an abnormality surrounding the conventional lesion. Also, note the small lesions visible on gM_0^A and f, which are not as clear on the T_1 and MTR maps.

0.02–0.03 for all of the brain tissues in both patients and controls. The estimates of the parameters produced also fit in generally with those presented previously (20), except where differences in technique and theory, such as the normalization of the experiment to produce an estimate of R, dictated otherwise.

Limited information about reproducibility was obtained from the single control subject imaged twice. The datasets were registered and 10 regions drawn in the white and gray matter. Analysis of the values obtained for each parameter in the two datasets showed changes in the parameters of 2.8% for T_1, 1.7% for f, and 2.2% for T_{2B}.

Analysis of Output

The different maps produced by this procedure are of varying value; for example, we found a value for RM_0^A greater than $10^5\ s^{-1}$ in all tissues in the brain. At these levels the SSQ and predicted signal intensity become independent of this parameter and the resulting parameter map is featureless. However, as can be seen in Fig. 2, other maps such as the bound proton fraction, f, $1/R_A T_{2A}$, and to a lesser extent T_2^B show brain structure and particularly lesions.

It can be seen from these maps that lesions show a reduction in both f and T_2^B compared with the surrounding NAWM; this, and the parameter estimates themselves, are in agreement with the preliminary data from this group (24,31) from an ROI analysis on a smaller cohort. Table 2 shows a comparison of the parameters produced by the fitting and the MTR in NAWM and MS lesions in the patient group along with the *P*-values produced from analysis using Student's paired *t*-test. The values compared are averages in each patient from a number of regions drawn in the lesions and NAWM. Table 3 shows a similar comparison, but this time between NAWM and white matter from the control group in a specific location. The values of f and MTR in these tables are given in percentage units (pu) as defined previously for MTR measurements (32).

Table 2
Values for the Parameters and Comparison Obtained From NAWM and MS Lesions

Parameter	NAWM (±SD)	MS lesions (±SD)	*P* value
$1/R_A T_2^A$	44 ± 3	28 ± 8	<0.001
$f/R_A(1-f)$ (s)	0.104 ± 0.002	0.101 ± 0.009	0.195
T_2^B (μs)	18.3 ± 0.4	15.9 ± 1.0	<0.001
f (pu)	14.0 ± 0.9	8 ± 2	<0.001
MTR (pu)	59 ± 1	55 ± 3	0.009

Table 3
Parameters Obtained From Patients and Volunteers Compared, Showing Significant Differences Between NAWM and White Matter in Controls for the Bound Proton Fraction, f

Parameter	NAWM	Control white matter	*P* value
$1/R_AT_2^A$	44 ± 5	43 ± 6	0.619
$f/R_A(1-f)$ (s)	0.105 ± 0.007	0.106 ± 0.007	0.814
T_2^B (μs)	18.0 ± 0.9	18.4 ± 0.5	0.259
f (pu)	14.0 ± 0.9	15.5 ± 0.7	0.018
MTR (pu)	59 ± 1	60 ± 3	0.399

These results come from comparison of regions drawn in right occipital white matter, but the pattern is repeated elsewhere in the white matter.

For comparison, analysis was also performed in the cortex to obtain data for this gray matter. From this analysis, gray matter has an f value, similar to lesions, of around 8 pu, with no difference seen between gray matter in controls and patients. Gray matter values of T_{2B} and $1/R_A T_{2A}$ are also reduced from NAGM values, although in the case of the former the reduction is only slight. Significant differences were seen between the $1/R_A T_{2A}$ values obtained from the controls and MS patients in gray matter, which is interesting, given that the same result is not seen in white matter.

Group-normalized whole-brain histograms of f for the patients and controls are shown in Fig. 3. The shape of the histograms seem to show subtle, yet clear, differences: the values at low f are higher in the patient group, as may be expected as lesions fall into this range. There is a corresponding decrease in the height of the patient histogram at higher values of f, suggesting the loss of the "extra" white matter seen in controls. This region also appears to contain a "kink" in the control histogram that is missing in the patients group, indicating that a more detailed analysis of this and the other parameter histograms may provide useful information. Comparisons of the peak height, peak location, and the 25th and 75th centile points between the MS subjects and controls were carried out using the independent samples *t*-test. Peak height did not differ between the two groups for any of the parameters tested ($P > 0.073$).

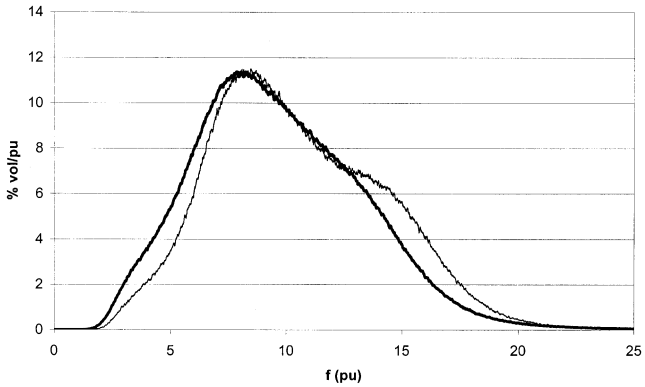

FIG. 3. Group histograms for the bound proton fraction, f. The thicker line represents the patient group (n = 20) and the thinner line the control group (n = 7). Note the increased height of the patient histogram at smaller values of f, due to the reduced value of f in NAWM and possibly the presence of lesions.

Peak location appears to be a slightly better discriminator, using this statistic there is a significant difference between the two groups in the $f/R_A(1-f)$ ($P = 0.015$) and MTR histograms ($P = 0.005$). However, it is the 25th centile point that gives the most impressive results, with $P = 0.01$, $P = 0.026$, $P = 0.041$, and $P = 0.002$ for the $f/R_A(1-f)$, f, $1/R_A T_{2A}$, and MTR histograms, respectively. Finally, the 75th centile point produced significant differences for f ($P = 0.028$) only. It should be noted that the histogram metrics described here are often correlated; however, four common measures were used to avoid the bias involved in the selection of a single metric. Also, unlike the differences seen between the parameter values from NAWM and MS lesions, none of these significances survive after application of the Bonferroni correction for multiple comparisons.

DISCUSSION

One area of interest in these results is the apparent improvement in the fit when using the Gaussian lineshape compared with the super-Lorentzian for the bound proton pool. This is contrary both to the work looking at postmortem samples by Henkelman and Morrison (17,20) and the in vivo studies presented by Sled and Pike (25). Although this is slightly surprising, there are a number of possible explanations. The most likely is that, as the super-Lorentzian demonstrated in Ref. 20 does not fit the data perfectly, a Gaussian form for the lineshape is a better approximation for the small range of data presented here. This would apply when comparing this work to any of that described above, as far fewer data points were collected for this work. This suggests that better estimates of the parameters may be made with an increase in the number of data points, although whether this would lead to significant differences in the parameters produced is not clear. It is accepted that choosing the Gaussian lineshape from a subset of the data used in the study proper may bias the results. However, as the Gaussian lineshape consistently fitted the data better than the other lineshapes, and given that there is limited data in this preliminary study, this was considered acceptable. Study of the choice of lineshape as a function of the number of data points acquired and the optimization of their location, however, is an important subject that is not addressed in this work.

Improvements in the implementation of the fitting routine and fixing the parameter RM_0^A would help reduce the long time required to produce the maps; this parameter appears to have very little variation between tissues and appears to give no useful information beyond the fact that

the two pools are well coupled. It should be noted that while this value is not comparable to values of R from other groups, as it has not been normalized to the native magnetization in a voxel to remove M_0^A from the model, the behavior of the parameter differs from that presented elsewhere (25). In that case, the parameter took much lower values and varied usefully throughout the brain. Interestingly, when RM_0^A is set to a value similar to that of Sled and Pike, the SSQ does vary with this parameter, although it is significantly higher than when the parameter takes a value $>10^5$. This suggests that there is a methodological difference causing a discrepancy in the fitted value of this parameter. One possibility is that the relative length of the MT pulse to TR is the cause of this problem; however, to cover all 28 slices in 1 TR, the length of the MT pulse cannot be increased without altering the receive bandwidth, which would reduce the SNR of the sequence. This lack of usefulness in the parameter RM_0^A is disappointing, but should be viewed in the context of obtaining whole-brain coverage.

The collection of whole-brain parameter maps for MS patients in a clinically acceptable time is a big step forward in the clinical development of qMT. The maps do not have the same quality as those published previously (25), in that there appears to be greater noise in the values of the parameters obtained from the fits. This is unsurprising, given that the resolution of the images is approximately doubled from 2×2 mm in Sled and Pike's (25) work to 1×1 mm here, with a reduction in the slice thickness from 7 to 5 mm. This results in a reduction of voxel volume from 28 mm^3 to 5 mm^3, which will reduce the SNR in the images. This and the reduced number of data points used in this work will introduce a greater uncertainty into the fitting procedure. However, to achieve full brain coverage at the chosen resolution in a similar time to the single slice imaged in (25), the number of data points acquired must be compromised. Despite this, the f map still shows the brain structure in good detail and in patients the lesions are clearly visible as having a reduced bound proton fraction. This is supported by the ROI analysis, which shows a significant reduction in f in lesions compared with the surrounding NAWM.

The quality of the fitting seems to be adequate to have faith in the parameters produced; this may be improved with refinements to the scanning procedure such as changes to the selection of data points, or to the fitting procedure such as refinements in the starting estimates of the parameters. The goodness of fit measures seem to be comparable to those presented in other work (20) and although the fitting of the maps is a little noisy, as mentioned above, the overall quality is still good enough to obtain meaningful comparisons about the behavior of the tissues. This is further backed up by the map of gM_0^A; this should simply be a measure of the PD in a tissue, so the fact that it shows clearly brain structure and is very similar to the PD-weighted images for producing the T_1 suggests that the fitting is working well.

Although reproducibility data was collected on only one subject, it is encouraging to see that the results are reproducible between scans. Although this experiment cannot give any information about the effects of movement or artifact on the fitting procedure, it does indicate that random effects such as noise do not seem to influence the fitted parameters greatly.

The pilot clinical results obtained are encouraging in that some of the parameters produced can be used to separate MS lesions from NAWM. Although, as can be seen, the same is true of the MTR, so it would be very surprising if this were not the case. If the significant differences between NAWM and white matter in controls are preserved in a larger group this would also be an interesting result, as it further indicates the involvement of all white matter in MS. This finding should not be too surprising, as differences are seen in other MR parameters such as fractional anisotropy and T_2 (33,34), but does further indicate that MS affects all white matter in the brain, not just that in which a lesion appears. It is true, however, that this result only shows significance at a less stringent threshold ($P = 0.018$) and may be an artifact of the differences in age between the groups, particularly as the control group is so small. That f appears to be a better discriminant than the MTR for these two tissues, however, is encouraging, although given that previous studies have found the MTR to separate NAWM and control white matter (35) the small group size may be responsible for a misleading result.

Similar arguments about the small group size are also applicable to the histogram analysis, which, combined with the fact that the Bonferroni correction suggests that there are no clear significant differences between the histograms from patients and volunteers, means that no firm conclusions can be draw from this analysis. However, it is encouraging that histograms of the various qMT parameters could be produced and that from analysis of the individual histograms, which is not shown here, that their shape is reproducible across subjects. It is interesting that $f/R_A(1-f)$ gives the most encouraging results from this basic analysis, as the map of this parameter does not seem as useful as its related parameter, f, as evidenced by a lack of as clear a brain structure. Whether histograms of the qMT parameters give more information than the conventional MTR histograms is certainly open to debate, as the results show as good, if not better, separation of control and patients using this measure. However, despite the limitations of the analysis performed here, the results indicate that there may be benefits to a larger, more complex study of histograms of the various parameters.

Figure 2 shows a number of interesting features. Several of the parameter maps show a number of white matter lesions, bilaterally in the centrum semiovale. These are best seen on the map of gM_0^A, or PD, but are also clear on the map of f. The brain structures are also clearly visible on these maps and to a lesser extent on the maps of $1/R_A T^2{}_A$, $f/R_A(1-f)$ and T_{2B}. The lesions are also visible on these maps, although the map of T_{2B} does not show several smaller lesions within the centrum semiovale, indicating that qMT is sensitive to lesion heterogeneity. Lesion age or structural differences may account for these variations, which may be investigated using the extra parameters imaged using this technique. It is also interesting to note that the MTR map shows the two larger lesions relatively clearly, but the smaller lesions are missing. In addition, there appears to be a discrepancy between the size and shape of the lesions in the left centrum semiovale; the PD

map seems to show two distinct lesions with different intensities, an effect mirrored in the T_1 map. However, the T_{2B} and $1/R_A T^2_A$ maps show only the more posterior of these two lesions; the f and $f/R_A(1-f)$ maps seem to show one larger lesion; while the MTR map falls somewhere in between. Quantitative analysis of the parameter maps in regions of NAWM, the large lesion visible on all maps and the small lesion occurring below it (which is only visible on some maps), confirm that there are large differences in the level of signal change in some of the parameters in these regions. In particular, it appears that there is an abnormality in f surrounding the larger lesion and that this information cannot be obtained by the conventional imaging techniques shown here. Also, the signal change in the smaller lesion varies between 9 and 31% for all qMT parameters except T_{2B}, where no change is seen, while the MTR only shows a change of 6% in intensity. A larger study is needed, however, to assess the sensitivity and specificity of these differences. More work is also needed to compare the overall utility of qMT to that of an optimized conventional MTR, taking into account any differences in attainable scan time, slice thickness, coverage, in-plane resolution, etc.

It is also interesting to look in detail at the parameter $1/R_A T_{2A}$. This parameter shows significant differences between NAWM and MS lesions and between gray matter in patients and controls. Although this finding is seen in a small group, it does indicate possible changes in the gray matter as well as the white matter of patients. However, if a typical T_{1A} time of 0.6 sec is assumed, then T_{2A} can be calculated to be around 14 ms for both NAWM and white matter in controls. Even allowing for the fact that T_{1obs} will be shorter than T_{1A}, this is much shorter than the typically accepted T_2 value of white matter, around 80–100 ms (36), which will be, if anything, slightly shorter than T_{2A}. To get a T_{2A} of this magnitude the value of T_{1A} would have to be around 4 sec. A similar result was noted by Morrison and Henkelman (20), who suggested that multicompartment relaxation made analysis of the component parts of this parameter unwise. It has been suggested that "partially bound" water broadens the lineshape of the free water, causing this discrepancy, and it may well be that the two-pool model used here and in the majority of similar work does not completely describe the interactions occurring; indeed, multicompartmental analysis of transverse relaxation times (37) has suggested that there are at least three water pools in brain tissues.

CONCLUSION

We have demonstrated a reliable method for estimating qMT parameters in the whole brain in a clinically acceptable time. Three of these parameters, f, $1/R_A T_{2A}$, and T_{2B}, appear to be physiologically specific and altered in MS lesions; in addition, f is also altered in NAWM. These parameters give additional information to MTR, as seen by the variable appearance of lesions on the parameter maps, and may be used to give improved tissue discrimination, as evidenced by the statistical tests described previously. We have also shown that histograms of some of these parameters may also show differences for some parameters between patients and controls.

ACKNOWLEDGMENTS

The authors thank the MS society of Great Britain and Northern Ireland for their support of this work and the NMR research unit.

REFERENCES

1. Edzes HT, Samulski ED. The measurement of cross-relaxation effects in the proton NMR spin-lattice relaxation of water in biological systems: hydrated collagen and muscle. J Magn Reson 1978;31:207–229.
2. Fung B. Nuclear magnetic resonance study of water interactions with proteins, biomolecules, molecules and tissues. In: Methods in enzymology, vol. 127. San Diego: Academic Press; 1986.
3. Pike GB. Pulsed magnetization transfer contrast in gradient echo imaging: A two-pool analytic description of signal response. Magn Reson Med 1996;36:95–103.
4. Adler RS, Swanson SD, Yeung HN. A three component model for magnetization transfer. Solution by projection-operator technique and application to cartilage. J Magn Reson 1996;110:1–8.
5. Forsen S, Hoffman RA. Study of moderately rapid chemical exchange reactions by means of nuclear magnetic double resonance. J Chem Phys 1963;39:2892–2901.
6. McGowan JC. The physical basis of magnetization transfer imaging. Neurology 1999;53:S3–S7.
7. van Buchem MA, Tofts PS. Magnetization transfer imaging. Neuroimag Clin N Am 2000;10:771–788.
8. Henkelman RM, Stanisz GJ, Graham SJ. Magnetization transfer in MRI: a review. NMR Biomed 2001;14:57–64.
9. Wolff SD, Balaban RS. Magnetization transfer contrast (MTC) and tissue water proton relaxation in vivo. Magn Reson Med 1989;10:135–144.
10. Dousset V, Grossman RI, Ramer KN, Schnall MD, Young LH, Gonzalezscarano F, Lavi E, Cohen JA. Experimental allergic encephalomyelitis and multiple-sclerosis-lesion characterization with magnetization transfer imaging. Radiology 1992;182:483–491.
11. Berry I, Barker GJ, Barkhof F, Campi A, Dousset V, Franconi JM, Gass A, Schreiber W, Miller DH, Tofts PS. A multicentre measurement of magnetisation transfer ratio in normal white matter. J Magn Reson Imag 1999;9:441–446.
12. Silver NC, Barker GJ, Miller DH. Standardisation of magnetisation transfer imaging for multicentre studies. Neurology 1999;53:S33–S39.
13. Filippi M, Iannucci G, Tortorella C, Minicucci L, Horsfield MA, Colombo B, Sormani MP, Comi G. Comparison of MS clinical phenotypes using conventional and magnetization transfer MRI. Neurology 1999; 52:588–594.
14. van Buchem MA, Udupa JK, McGowan JC, Miki Y, Heyning FH, BoncoeurMartel MP, Kolson DL, Polansky M, Grossman RI. Global volumetric estimation of disease burden in multiple sclerosis based on magnetization transfer imaging. Am J Neuroradiol 1997;18:1287–1290.
15. Ge YL, Grossman RI, Udupa JK, Babb JS, Mannon LJ, McGowan JC. TI Magnetization transfer ratio histogram analysis of normal-appearing gray matter and normal-appearing white matter in multiple sclerosis. J Comput Assist Tomogr 2002;26:62–68.
16. Dehmeshki J, Ruto AC, Arridge S, Silver NC, Miller DH, Tofts PS. Analysis of MTR histograms in multiple sclerosis using principal components and multiple discriminant analysis. Magn Reson Med 2001; 46:600–609.
17. Henkelman RM, Huang X, Xiang Q, Stanisz GJ, Swanson SD, Bronskill MJ. Quantitative interpretation of magnetization transfer. Magn Reson Med 1993;29:759–766.
18. Quesson B, Thiaudiere E, Delalande C, Dousset V, Chateil JF, Canioni P. Magnetization transfer imaging in vivo of the rat brain at 4.7 T: interpretation using a binary spin-bath model with a super-Lorentzian lineshape. Magn Reson Med 1997;38:974–980.
19. Yeung HN, Adler RS, Swanson SD. Transient decay of longitudinal magnetization in heterogeneous spin systems under selective saturation. IV. Reformulation of the spin-bath-model equations by the Redfield-Provotorov theory. J Magn Reson A 1994;106:37–45.
20. Morrison C, Henkelman RM. A model of magnetization transfer in tissues. Magn Reson Med 1995;33:475–482.
21. Pike GB, Glover GH, Hu BS, Enzmann DR. Pulsed magnetization transfer spin-echo imaging. J Magn Reson Imag 1993;3:531–539.
22. Chai JW, Chen C, Chen JH, Lee SK, Yeung HN. Estimation of in vivo proton intrinsic and cross relaxation rate in human brain. Magn Reson Med 1996;36:147–152.

23. Yarnykh VL. Pulsed Z-spectroscopic imaging of cross-relaxation parameters in tissues for human MRI: theory and clinical applications. Magn Reson Med 2002;47:929–939.
24. Ramani A, Dalton C, Miller DH, Tofts PS, Barker GJ. Precise estimate of fundamental in-vivo mt parameters in human brain in clinically feasible times. Magn Reson Imag 2002;20:721–731.
25. Sled JG, Pike GB. Quantitative imaging of magnetization transfer exchange and relaxation properties in vivo using MRI. Magn Reson Med 2001;46:923–931.
26. Ramani A, Tofts PS. Comparison of continuous wave theory to pulsed multicenter MT data. In: Proc 8th Annual Meeting ISMRM, Denver, 2000.
27. Parker GJ, Barker GJ, Tofts PS. Accurate multislice gradient echo *T*(1) measurement in the presence of non-ideal RF pulse shape and RF field nonuniformity. Magn Reson Med 2001:45:838–845.
28. Studholme C, Hill DLG, Hawkes DJ. An overlap invariant entropy measure of 3D medical image alignment. Pattern Recognit 1999;32:71–86.
29. Ford B, Bentley J, Du Croz JJ, Hague SJ. The NAG library 'machine'. Softw Pract Exp 1979;9:65–72.
30. Numerical Algorithms Group. http://www.nag.com/
31. Dalton CM, Ramani A, Wheeler-Kingshott C, Barker GJ, Miller DH, Tofts PS. Bound water magnetization transfer measurements in patients with multiple sclerosis: a pilot study. In: Proc 10th Annual Meeting ISMRM, Hawaii, 2002.
32. Barker GJ, Tofts PS, Gass A. An interleaved sequence for accurate and reproducible clinical measurement of magnetization transfer ratio. Magn Reson Imag 1996;14:403–411.
33. Guo AC, MacFall JR, Provenzale JM. Multiple sclerosis: diffusion tensor MR imaging for evaluation of normal appearing white matter. Radiology 2002;222:729–736.
34. Goodkin DE, Rooney WD, Sloan R, Bacchetti P, Gee L, Vermathen M, Waubant E, Abundo M, Majumdar S, Nelson S, Weiner MW. A serial study of new MS lesions and the white matter from which they arise. Neurology 1998;51:1689–1697.
35. Ropele S, Strasser-Fuchs S, Augustin M, Stollberger R, Ezinger C, Hartung HP, Fazekas F. A comparison of magnetization transfer ratio, magnetization transfer rate, and the native relaxation time of water protons related to relapsing-remitting multiple sclerosis. Am J Neuroradiol 2000;21:1885–1891.
36. Stevenson VL, Parker GJM, Barker GJ, Birnie K, Tofts PS, Miller DH, Thompson AJ. Variations in T1 and T2 relaxation times of normal appearing white matter and lesions in multiple sclerosis. J Neurol Sci. 2000;178:81–87.
37. Whittall KP, MacKay AL, Graeb DA, Nugent RA, Li DKB, Paty DW. In vivo measurement of T-2 distributions and water contents in normal human brain. Magn Reson Med 1997;37:34–43.